J. Wind Eng. Ind. Aerodyn. 98 (2010) 345–352

Contents lists available at ScienceDirect

Journal of Wind Engineering and Industrial Aerodynamics

journal homepage: www.elsevier.com/locate/jweia

Wind tunnel investigation of an ICE 3 endcar on three standard ground scenarios

Martin Schober [a,*], Marco Weise [a], Alexander Orellano [a], Peter Deeg [b], Wolfgang Wetzel [c]

[a] Center of Competence Aerodynamics and Thermodynamics, Bombardier Transportation, Am Rathenaupark, 16761 Hennigsdorf, Germany
[b] Deutsche Bahn AG, DB Systemtechnik Aerodynamic Measurements, Völckerstraße 5, 80939 München, Germany
[c] Siemens Transportation Systems, Locomotives TS LM D CoT Krauss-Maffei-Str. 2, 80997 München, Germany

ARTICLE INFO

Article history:
Received 9 March 2009
Received in revised form
11 December 2009
Accepted 14 December 2009
Available online 21 January 2010

Keywords:
Cross wind
Aerodynamics
Train
Wind tunnel
Ground simulation

ABSTRACT

An ICE 3 model has been investigated in an automotive wind tunnel on three different ground configurations by means of force measurements and tuft flow visualisations. The aerodynamic force and moment coefficients reveal a strong dependency on the ground configuration, with the embankment configuration giving the highest measured coefficients only for yaw angles $\beta < 40^{\circ}$. The coefficients obtained through the Baker hypothesis are found to be larger than those measured directly on the embankment. The poor agreement between the "measured on embankment coefficients" and the "flat ground with Baker transformation coefficients" is attributed to the fundamental mismatch of relative flow velocities between wind, train and ground during the wind tunnel measurements with the train situated on the embankment. The mismatch of flow velocities causes a strong longitudinal vortex on the leeward side of the embankment which does not exist in reality and significantly alters the overall flow field.

It is thus recommended, for the determination of aerodynamic forces acting on a train on an embankment, to measure the aerodynamic coefficients for the flat ground configuration and subsequently apply the Baker hypothesis.

1. Introduction

The aerodynamics of a train under the influence of cross winds is a safety relevant topic which is covered in European legislation within the framework of the Technical Specification for Interoperability (TSI) (EC, 2006), in the European Norm prEN14067-6 (CEN, 2008) as well as in national standards in the UK (Blakeney, 2000) and in Germany (DB Netz AG, 2006).

The modelling of cross wind acting on a train inside a wind tunnel represents a challenge due to the differing ground scenarios, e.g. flat ground corresponding to the situation on flat ground and on bridges, ballast and rail corresponding to regular tracks as well as the special case of high embankments (cf. Figs. 1 and 2). The modelling is especially complicated due to the differing relative speeds and yaw angles between the wind and the train on one side and the wind and the ground on the other side. Especially the lift force has been found by Baker and Humphreys (1996) to be sensitive to the Reynolds number and in particular to the ground simulation in the wind tunnel.

In addition to the ground modelling difficulties, the Reynolds number of modern high speed trains based on train width and a cruising speed of 350 km/h is approximately $Re = 2 \times 10^7$ and imposes a further challenge for most conventional wind tunnels. The abilities of computational fluid dynamics (CFD) to handle these challenges are comprehensively described by Diedrich et al. (2007).

The principal approaches for the experimental modelling of the above-mentioned relative movements and yaw angles are as follows:

1. Placing the train model onto a stationary flat ground, e.g. neglecting both the relative movement between ground and train as well the infrastructure (such as an embankment).
2. Placing the train model onto a standardised 1 m ballast and rail configuration, e.g. neglecting the relative movement between ground and train, but considering the "nearest" part of the infrastructure.
3. Placing the train model onto an embankment, e.g. neglecting the relative movement between ground and train but considering the infrastructure.
4. Placing the train model onto a moving belt, e.g. neglecting the infrastructure, but considering the relative movement between ground and train.

* Corresponding author.
E-mail address: Martin.Schober@de.transport.bombardier.com (M. Schober).

0167-6105/$ - see front matter © 2009 Elsevier Ltd. All rights reserved.
doi:10.1016/j.jweia.2009.12.004

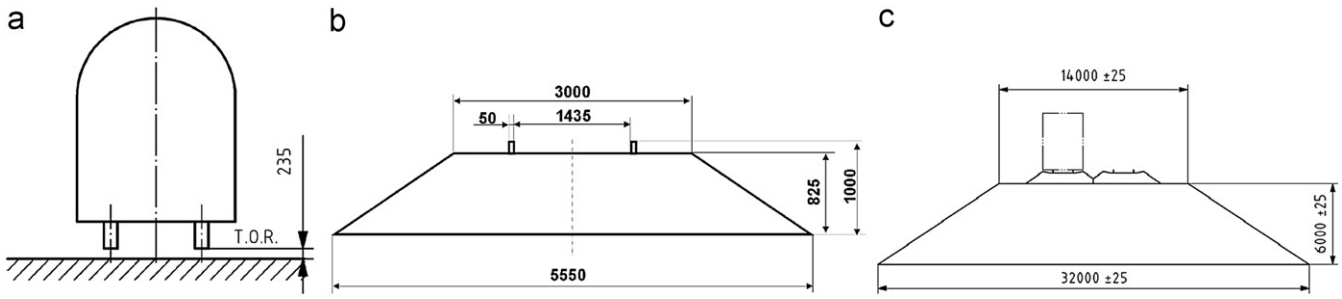

Fig. 1. Tested wind tunnel ground configurations CEN, 2008: (a) true flat ground, (b) ballast and rail flat ground, (c) 6 m embankment.

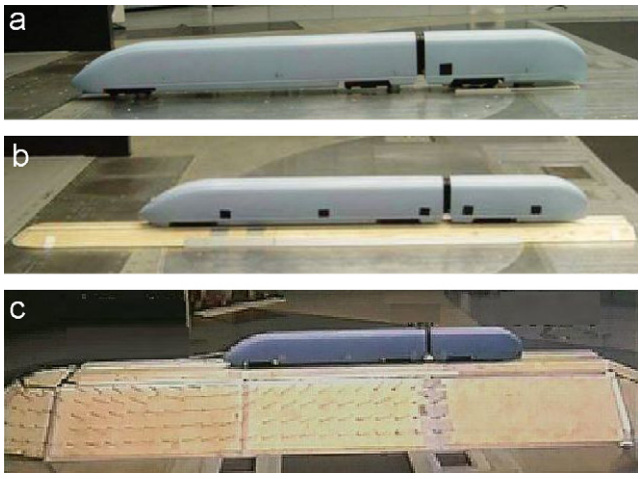

Fig. 2. ICE 3 on (a) flat ground, (b) ballast and rail, (c) 6 m embankment.

5. Shooting the train model on an embankment across a wind tunnel, e.g. considering both the relative movement between ground and train as well as considering the infrastructure.

While the last method certainly is the most proper method with respect to the correct representation of relative movements and infrastructure, the problems with respect to too small Reynolds numbers, unsteady force measurements and track (guide way) irregularities affecting the aerodynamic force measurements have prevented this approach from being commonly used in the past.

The present study investigates the influence of three stationary ground configurations in a wind tunnel on the measured aerodynamic coefficients of a modern high-speed train.

2. Experimental setup

A scale 1:15 model of an ICE 3 has been investigated in the Audi aero-acoustic wind tunnel. The wind tunnel is a closed loop type tunnel with a 3/4 open test section and features a boundary layer suction through a perforated floor directly at the nozzle exit, which was switched on during the measurements. The maximum wind-tunnel speed is 280 km/h, corresponding to 78 m/s at the exit of the 4 m × 2.8 m nozzle, yielding a Reynolds number of 1×10^6 based on the vehicle's characteristic length of $l = 3\,\mathrm{m}/15$. The turbulence intensity of the free stream flow is $Tu_x \leq 0.3\%$, deviation from block profile is $\Delta u/u_\infty \leq 1\%$ and angularity is better than 2°. The models and ground configurations were installed on a turn table laid out for automotive scale 1:4 models located on the centre line of the test section, directly downstream of the nozzle. The maximum blockage of the test section by the tested models does not exceed $B = 3.8\%$ for yaw angles up to 30° and $B = 6.1\%$ for yaw angles up to 90°. An external RUAG (Type 192) balance, mounted directly underneath the ground simulation, has been used. An internal mounting was not feasible due to the limited space inside the scale 1:15 model. The use of the wind tunnel scale 1:1 external balance was not appropriate due to insufficient resolution of the forces and moments. The ground configurations on which the ICE 3 was investigated are shown in Figs. 1 and 2:

- A *flat ground—FG* configuration with a gap of 235 mm (full scale) between the wheels and the ground (according to TSI HS RST, EC, 2006 and RIL 80704, DB Netz AG, 2006).
- A *single-track ballast and rail—STBR* configuration with a height of 1 m (full scale) (according to prEN14067-6).
- An *embankment—EMB* configuration with a total height of 6 m (full scale) featuring double track ballast and rails (according to TSI HS RST, EC, 2006).

3. Results

3.1. Tuft visualisation on an embankment

Fig. 3 shows tuft visualisations on the windward side of the embankment at yaw angles of 0°–30°. For small yaw angles of 0° and 10°, the tufts are directed in parallel with the wind tunnel floor and the embankment. For the higher yaw angles of 20° and 30°, the flow field on the windward side becomes directed upwards, thereby altering the pitch angle of the approaching flow relative to the train on top of the embankment. When viewed from the front in Fig. 3e, a change of flow direction near the leading edge of the embankment is clearly visible, highlighting the effect of the presence of the embankments nose shape. In addition, a three-dimensional pattern is exhibited upstream of the train revealing the footprint of a longitudinal vortex on the leeward side (also visible on side view at 40° shown in Fig. 2c).[1]

3.2. Force coefficients

The force and moment coefficients according to the EN14067 coordinate system (Fig. 4) and Eqs. (1)–(6) of the ICE 3 are shown in Fig. 5 and tabulated in Appendix A. The results have been checked to be nearly independent of Reynolds number (cf. Section 3.2.1). In addition to the directly measured aerodynamic properties on flat ground (FG), single-track ballast and rail (STBR) and the 6 m high embankment (EMB), calculated coefficients for the embankment case using the "Baker hypothesis" (Baker, 1985) (cf. Section 3.3 for details) based on

[1] This effect can be minimised by extending the embankment further upstream to the nozzle exit, however, at the cost of interference problems between wind tunnel nozzle and embankment.

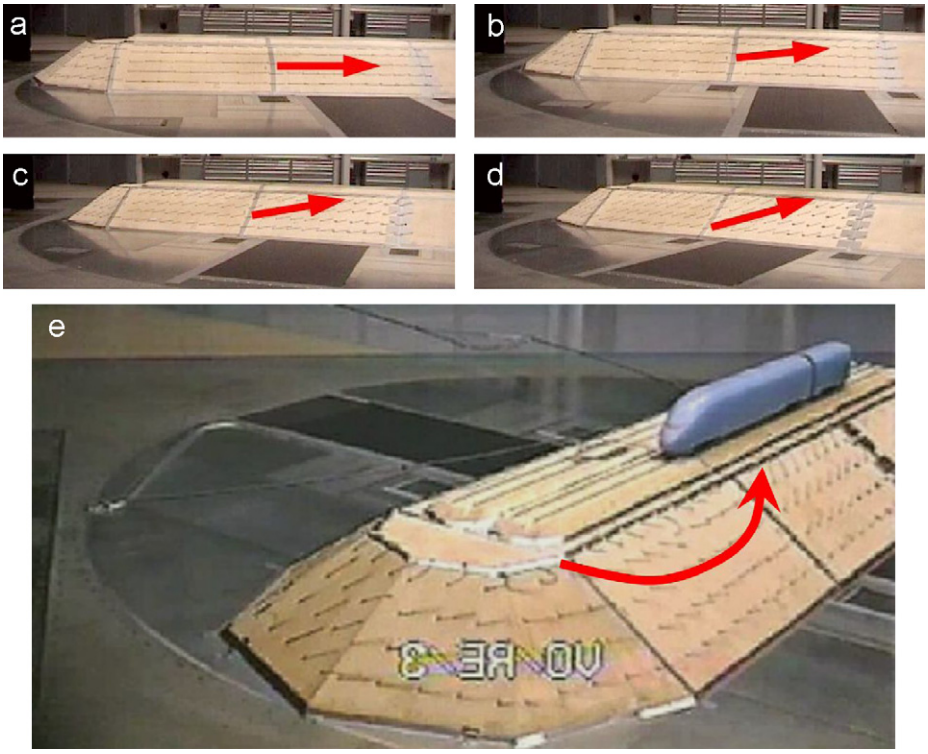

Fig. 3. Flow structure on the windward side of an embankment at (a) 0°, (b) 10°, (c) 20°, (d) 30° and on the leeward side at (e) 40°.

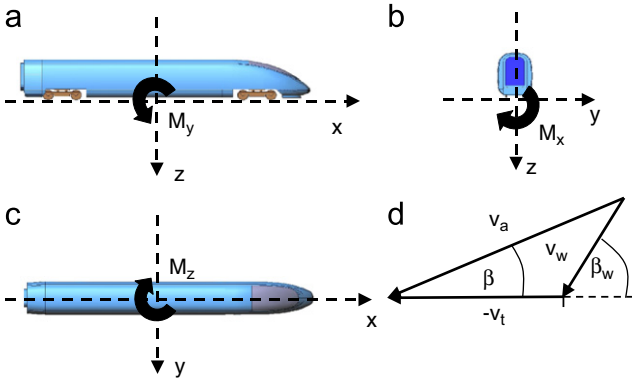

Fig. 4. Coordinate system according to EN14067-1, (a) side view, (b) rear view, (c) top view, (d) velocity triangle (CEN, 2008).

flat ground (EMB Baker (FG)) and ballast and rail data (EMB Baker (STBR)) are shown. The most important parameter with respect to cross-wind stability is the roll-moment coefficient around the leeward track c_{mxlee}, which is shown in Fig. 5g. It can be noted that the flat ground results are considerably below those obtained on the ballast and rail configuration. The measured coefficients on the 6 m embankment are above the ballast and rail results for yaw angles below 40°, but drop significantly below those of ballast and rail for yaw angles above 40°:

$$F_x = c_x A \tfrac{1}{2}\rho v_a^2 \quad \text{(Drag)} \tag{1}$$

$$F_y = c_y A \tfrac{1}{2}\rho v_a^2 \quad \text{(Side force)} \tag{2}$$

$$F_z = c_z A \tfrac{1}{2}\rho v_a^2 \quad \text{(Lift)} \tag{3}$$

$$M_x = c_{mx} A l \tfrac{1}{2}\rho v_a^2 \quad \text{(Roll)} \tag{4}$$

$$M_y = c_{my} A l \tfrac{1}{2}\rho v_a^2 \quad \text{(Pitch)} \tag{5}$$

$$M_z = c_{mz} A l \tfrac{1}{2}\rho v_a^2 \quad \text{(Yaw)} \tag{6}$$

$$c_{mxlee} = c_{mx} - c_z \frac{b_a}{2l} \quad \text{(Roll moment coefficient around leeward track)} \tag{7}$$

$$A = 10\,\text{m}^2, \quad l = 3\,\text{m}, \quad b_a = 1.5\,\text{m (full scale)} \tag{8}$$

3.2.1. Reynolds number dependency

A Reynolds number check performed at $0.5 \times Re_{max}$ and $0.75 \times Re_{max}$ according to the wind tunnel specification provided by TSI HS RST (EC, 2006) and prEN14067-6 (CEN, 2008) is shown in Fig. 6. The Reynolds number is based on the characteristic length $l = 3$ m (full scale).

The change of $c_{mxlee}(30°)$ with increasing Reynolds number is below 3% for all investigated cases. Interestingly, $c_{mxlee}(30°)$ decreases with increasing Reynolds number for the true flat ground and the ballast and rail configuration, but increases for the embankment configuration. The reason for these opposing trends remains unknown.

3.2.2. True flat ground versus ballast and rail flat ground

As already mentioned and described in detail in the preliminary norm prEN 14067-6 (CEN, 2008), there exist two interpretations of a "flat ground" setup for train aerodynamics:

The "true flat ground—FG" configuration consists of a train located above a flat plate, i.e. in the absence of any rail or ballast detail. For historical reasons, the distance between the wheel–rail contact point and the plate is set to 235 mm (full scale). This elevation approximately corresponds to the height of the rail and the sleeper, thus would yield the proper under body blockage in the wind tunnel at 0° yaw angle. The main advantage of this setup

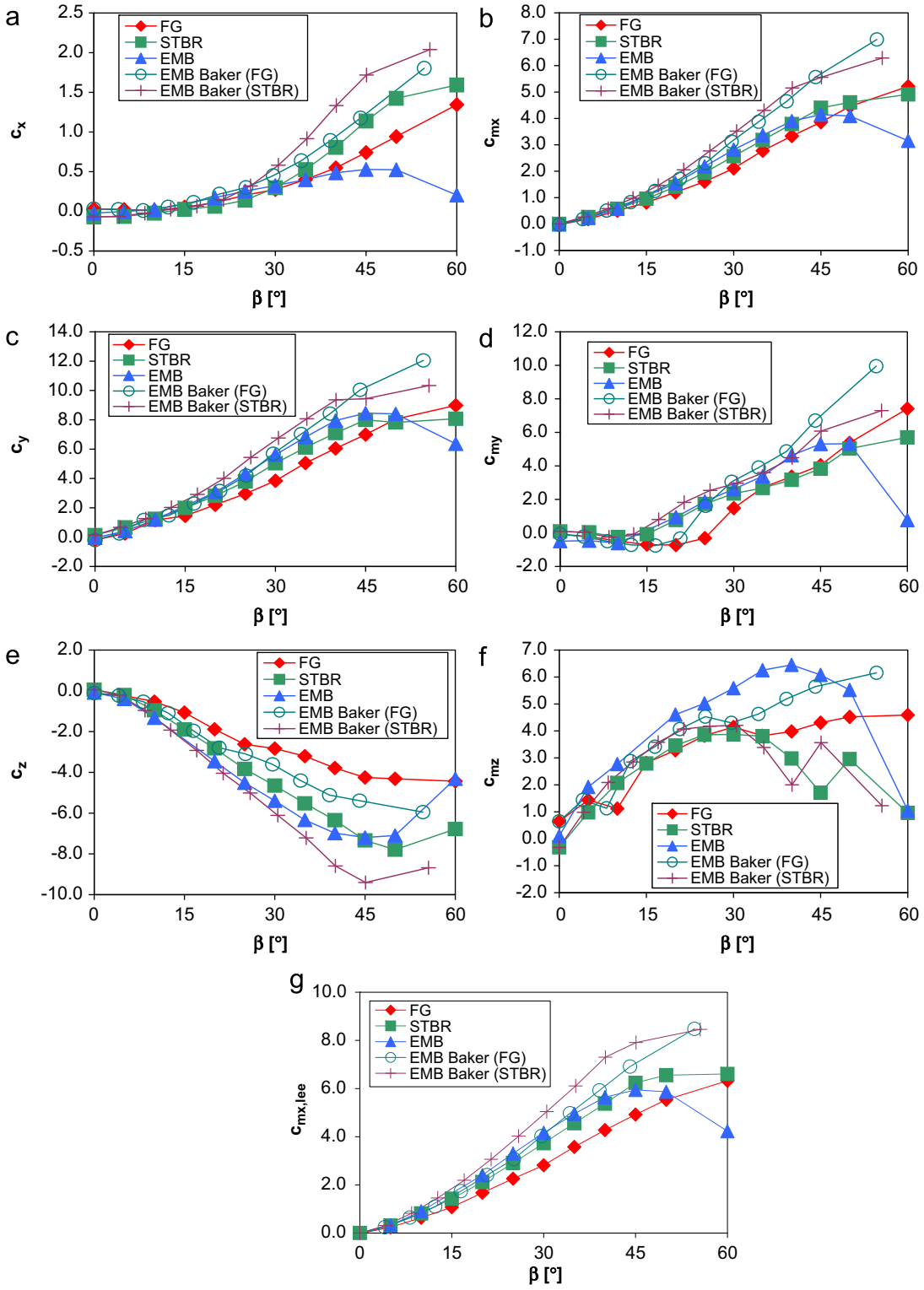

Fig. 5. Aerodynamic coefficients of an ICE 3 on different ground configurations.

is its extreme simplicity, the main shortcoming is an improper representation of the under belly flow field in yawed conditions.

The "*single-track ballast and rail—STBR*" configuration includes a simplified and standardised 1 m ballast bed with rails, but without any further details such as sleepers. The wheel–rail contact point is set to its proper value, thus the wheels usually need to be flattened in order to avoid real wheel–rail contact during the force measurements. The main advantages are its improved representation of the under belly flow field during cross wind and an attenuation of the wind tunnel boundary layer details, the main shortcomings are an increased experimental effort and the improper flow around the ballast bed itself (see Sections 3.3 and 4.1). This latter effect of introducing again the

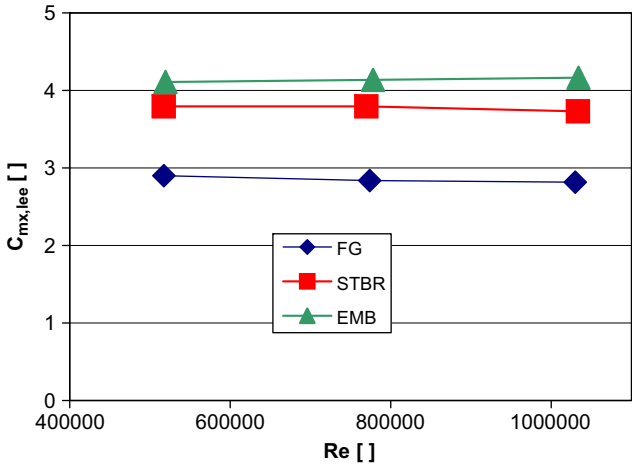

Fig. 6. Reynolds number check of $c_{mxlee}(30^{\circ})$ according to prEN140674-6 (CEN, 2008).

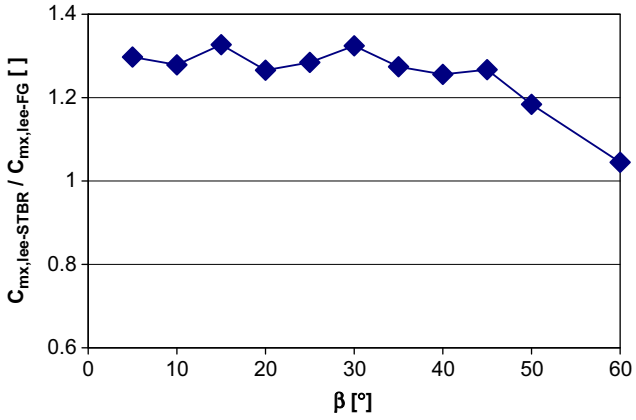

Fig. 7. Scaling factor between true flat ground and ballast and rail flat ground.

improper relative flow speeds across the ballast, however, is relatively small due to the small height of only 1 m (full scale) compared to the 7 m height of the standard "6 m embankment".[2]

For the sake of comparability and cost saving due to avoiding multiple wind tunnel tests, the prEN 14067-6 working group members are pushing forward the 1 m ballast and rail configuration, as it is seen more beneficial to improve the underbelly flow representation for cross wind at the expense of a slightly more complicated set up. Since there exists a large amount of experimental data for the true flat ground configuration, it would be desirable to determine an approximate scaling function to convert the existing "true flat ground" data into the "ballast and rail" configuration.

Due to the aforementioned physical differences between these two configurations, such a scaling can only be relatively crude. However, if this scaling function is determined for a variety of trains that differ significantly in shape and underbelly layout, one would at least be enabled to generate a worst-case scaling function.

Fig. 7 shows the scaling factor between the lee-rail rolling moment coefficient of the ballast and rail and the true flat ground configuration. The scaling factor is approximately 1.3 within the yaw angle range $5^{\circ} \le \beta \le 45^{\circ}$. For yaw angles above 45° the scaling factor decreases to 1.05 at 60°. Since the relevant yaw angle range for a high speed train is approximately $10^{\circ} \le \beta \le 30^{\circ}$ (cf. Orellano and Schober, 2006), the scaling factor of the investigated ICE 3 can be assumed to be constant and 1.3 within the range of interest.

3.3. *Transformation of the flat ground results to the 6 m embankment*

Baker (1985) investigated in detail the acceleration of the natural wind across an embankment (without any train) with both wind tunnel and track site measurements. He found, for wind angles between 90° (i.e. perpendicular to the embankment) and 30°, only the embankment-normal velocity component to be accelerated across the embankment (cf. Section 4.1), whilst the embankment-parallel component remained unchanged (cf. Fig. 8). This subsequently changes the local wind angle β_{EMB} on top of the embankment. The resulting wind velocity U_{EMB} is given by

$$U_{EMB} = \sqrt{(v_t + U_{WT}\cos\beta_{WT})^2 + f_{EMB,FG}^2 (U_{WT}\sin\beta_{WT})^2} \tag{9}$$

$$\beta_{EMB} = \arctan\left(\frac{f_{EMB,FG} U_{WT}\sin\beta_{WT}}{v_t + U_{WT}\cos\beta_{WT}}\right) \tag{10}$$

where $f_{EMB,FG}$ is the over-speeding coefficient, β_{WT} is the direction of the wind-tunnel flow relative to the embankment and β_{EMB} is the local wind angle on top of an embankment.

For the transformation of true flat ground measurements to data on an embankment, the train speed must be set to $v_t = 0$ since there is no relative movement between the train model and the wind-tunnel floor. Apparently, Eqs. (9) and (10) reduce to

$$\frac{U_{EMB}}{U_{WT}} = \sqrt{\cos^2\beta_{WT} + f_{EMB,FG}^2 \sin^2\beta_{WT}} \tag{11}$$

$$\tan\beta_{EMB} = f_{EMB,FG}\tan\beta_{WT} \tag{12}$$

For the conversion of flat ground data into embankment data it is assumed that the local wind speed U_{EMB} and the corresponding wind angle β_{EMB} on top of the embankment are equal to the values measured in the flat-ground experiment:

$$\beta_{WT,FG} = \beta_{EMB} \tag{13}$$

$$U_{WT,FG} = U_{EMB} \tag{14}$$

Thus, Eq. (11) is rewritten such that β_{EMB} is used as an argument:

$$\frac{U_{WT}}{U_{EMB}} = \sqrt{\cos^2\beta_{EMB} + f_{EMB,FG}^{-2} \sin^2\beta_{EMB}} \tag{15}$$

Assuming that in case the local wind speed and wind angle agree, the measured forces on the embankment and in the flat ground setup are the same, permits the scaling of the measured flat ground coefficients to the embankment case. In this case Eq. (15) can be applied to the aerodynamic forces and moments (cf. Eqs. (1)–(6))

$$C_{i,EMB}(\beta_{WT}) = C_{i,FG}(\beta_{EMB}) \frac{1}{\cos^2\beta_{EMB} + f_{EMB,FG}^{-2}\sin^2\beta_{EMB}} \tag{16}$$

$$i \in \{x, y, z, mx, my, mz, mxlee\} \tag{17}$$

For the transformation of the flat ground coefficients to the embankment coefficients, a value of $f_{EMB,FG} = 1.23$ has been used according to the RIL 80704 (DB Netz AG, 2006).

This procedure is henceforth called application of the "Baker hypothesis". According to Baker (1985) this transformation is only valid for wind angles $\beta_{WT} \ge 30^{\circ}$. It should be noted that when converting ballast and rail measurements into embankment data,

[2] The standard 6 m embankment has an additional 1 m ballast and rail ground added on top of the base 6 m (cf. Fig. 1).

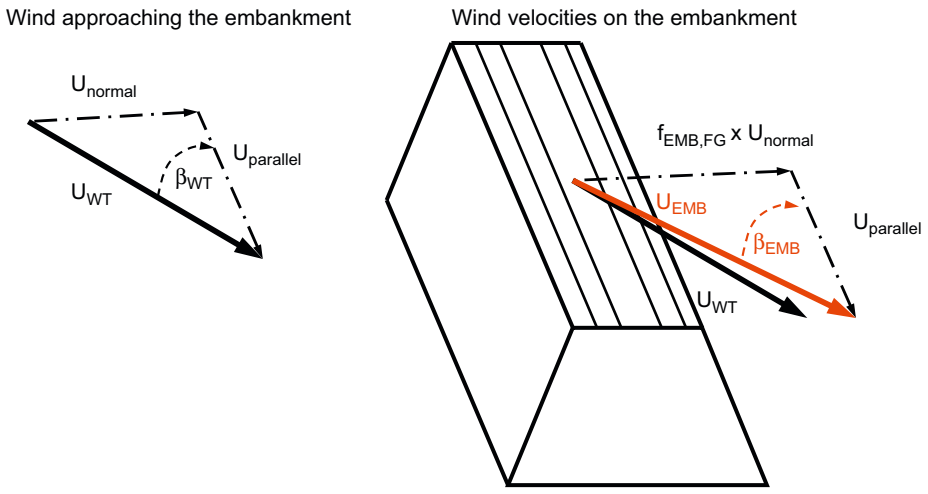

Fig. 8. Wind velocity components near and on an embankment.

the Baker coefficient $f_{STBR,FG} = 1.035$ valid for a 1 m standard ballast and rail configuration hast to be taken into account. Therefore, the conversion is done using an overall coefficient of $f_{EMB,STBR} = 1.23/1.035 = 1.188$ in this case.

The agreement between the "measured on embankment coefficients" and the "flat ground with Baker transformation coefficients" in Fig. 5 is rather poor. The large discrepancies at wind angles β_{WT} above 30° (valid range of "Baker hypothesis") are attributed to the fact that the flow around the embankment in the wind tunnel experiment significantly differs from the full scale reality (cf. Gawthorpe, 1994). For wind angles β_{WT} below 40° the impact of the leading edge of the embankment on the local flow field at the train model is so dominant that the measurements are significantly violated. It thus cannot be expected that the measured values agree with any real case with an arbitrarily long embankment ahead of the vehicle.

The coefficients obtained through the Baker hypothesis are generally larger than those measured directly on the embankment, suggesting that the wind tunnel approach enforced by the TSI HS RST (EC, 2006) requesting "measured on embankment coefficients" is not conservative. Whilst this lack of conservatism is only of minor importance within the TSI itself due to the TSI approach being based on a comparison to a reference vehicle under the same experimental conditions, this lack of conservatism has to be carefully evaluated as soon as an approach is based on actual risk analyses (Blakeney, 2000).

4. Discussion

4.1. The flow of wind over a skewed obstacle

A generic embankment, as it has been used in wind tunnel studies, has many similar features to "generic flow configurations", such as the backward-facing step or the fence, where a variety of publications exist. For example, Fernholz et al. (1993) showed that the flow behind a skewed backward facing step (cf. Fig. 9a) shows three regions (cf. Fig. 9b) that depend on the skewing angle α.[3] These three regions are dominated by either the step-normal, the step-parallel or both velocity components and exhibit quite different flow features:

2-D perpendicular: A "quasi-two-dimensional" separation for skew angles of 0° to approximately 30°. Here, the independence principle of Prandtl is valid, i.e. the transversal flow properties are independent of the stream-wise and wall-normal velocity components. Flow features as for instance the separation length, scale with the velocity component normal to the step.

2-D parallel: A "quasi-two-dimensional" separation for skew angles of 50° to approximately 90°, which is dominated by a strong longitudinal vortex immediately behind the step. Flow features as the separation length are dominated by the velocity component parallel to the step.

3-D: A "strongly three-dimensional" separation for skew angles of 30° to approximately 50°, where a transition between the above two patterns takes place, i.e. the flow field depends on both step normal- and parallel component.

Orellano and Schober (2003) showed that for modern high speed trains the wheel unloading due to cross wind is strongest for yaw angles β of 10°–30°. Due to the large velocity of the train ($v_{train} \approx 100$ m/s) relative to the ground, this corresponds to nearly perpendicular wind relatively to the track (80–90°) at a wind speed of approximately 30 m/s.

We therefore can conclude that for the real operation of a train, the characteristic velocity corresponds to the train speed and the dominant flow feature is the longitudinal vortex generated on the leeward side of the train. For the real flow across an embankment, in contrast, the characteristic velocity is the wind velocity, the angle of attack is nearly perpendicular and the flow is quasi-two-dimensional. In other words, the train's flow is "2-D parallel" whereas the flow across the embankment is "2-D perpendicular" in reality.

Within a wind-tunnel experiment with stationary embankment, the embankment is subject to nearly the same angle of attack and flow speed as the train and therefore, is also subject to a strong longitudinal vortex (see Fig. 2c) that is not present under real operational conditions. A separation of the velocity into components normal- and parallel to the embankment (Prandtl's decomposition) is not possible in the yaw angle range under consideration. In other words, both the train's and the embankment's flow are treated "2-D parallel" in the wind tunnel, which is inherently incorrect as far as the embankment is concerned.

5. Conclusion

An ICE 3 model has been investigated in an automotive wind tunnel on three different ground configurations by means of force

[3] Note that $\alpha = 90° - \beta$.

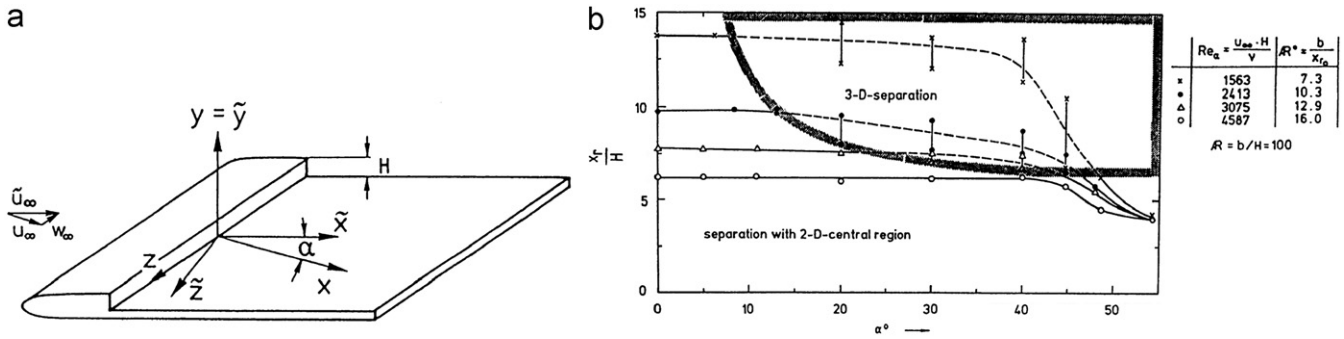

Fig. 9. The flow around a swept backward facing step (Fernholz et al., 1993).

measurements and tuft flow visualisations. The aerodynamic force and moment coefficients reveal a strong dependency on the ground configuration, with the embankment configuration giving the highest measured coefficients only for yaw angles $\beta < 40^{\circ}$. The coefficients obtained through the Baker hypothesis are found to be larger than those measured directly on the embankment, suggesting that the approach utilising an embankment inside the wind tunnel is not conservative. The poor agreement between the "measured-on-embankment coefficients" and the "flat-ground-with-Baker-transformation coefficients" is attributed to the fundamental mismatch of relative flow velocities between wind, train and ground during the wind tunnel measurements with the train situated on the embankment. The mismatch of flow velocities causes a strong longitudinal vortex on the leeward side of the embankment which does not exist in reality and significantly alters the overall flow field. Furthermore, the leading edge of the wind-tunnel embankment disturbs the flow field at small wind angles β_{WT} up to 40° and thus, violates the measurements.

It is thus recommended, for the determination of aerodynamic forces acting on a train on an embankment, to measure the aerodynamic coefficients for the flat ground configuration and subsequently apply the Baker hypothesis.

Appendix A. Measured aerodynamic coefficients of an scale 1:15 ICE 3 model

The force and moment coefficients according to the EN14067 coordinate system and Eqs. (1)–(6) of the ICE 3 are tabulated in Table 1.

Appendix B. Upstream length of ballast and rail

When using a ballast and rail flat ground set up, in addition to the cross section also the necessary upstream length of the ballast and rail needs to be determined. The essential requirement is that the upstream part needs to be sufficiently long to generate a nearly two-dimensional flow with respect to the train. As has been discussed in Section 4.1, this is generally not possible. However, since the height of the ballast and rail is small (approximately only 1/4 of the train height), the influence of the ballast and rail on the three-dimensional character of the flow is small compared to that of the train itself.

In order to assess the necessary upstream length, the impact on the lee rail moment coefficient, cmxlee, was checked in a separate wind tunnel campaign with a scale 1:10 train model of a driving trailer. Fig. 10a shows a sketch of the experimental set up. Two different upstream ballast lengths of $2 \times h$ and $7 \times h$, with h being the vehicle height, were investigated. The first ground configuration is denoted "short ballast and rail", the latter "long ballast and rail".

Fig. 10 b shows the evolution of the relative lee rail moment coefficient $c_{mxlee}/c_{mxlee,max}$ for the two different ballast lengths. The difference between the two curves is negligible. An upstream ballast length of two train heights h or 8 m full scale can thus be considered as sufficient for wind tunnel experiments.

Table 1
Coefficients of an ICE 3 scale 1:15 model measured in the Audi wind tunnel on true flat ground (FG), ballast and rail flat ground (STBR) and a 6 m standard embankment (EMB) according to the specification provided by TSI HS RST (EC, 2006) and prEN14067-6 CEN, 2008.

	Aerodynamic coefficients						
β (°)	c_x (−)	c_y (−)	c_z (−)	c_{mx} (−)	c_{my} (−)	c_{mz} (−)	c_{mxlee} (−)
FG							
0	0.0310	−0.2003	−0.1125	−0.0226	−0.0730	0.6491	−0.0226
5	0.0234	0.2500	−0.2340	0.1844	−0.2159	1.4379	0.2430
10	0.0102	1.1559	−0.5285	0.5060	−0.4898	1.1194	0.6381
15	0.0531	1.4476	−1.0658	0.8109	−0.6989	2.8166	1.0774
20	0.1081	2.2019	−1.8848	1.2016	−0.7253	3.2819	1.6728
25	0.2044	2.9591	−2.6202	1.6061	−0.3105	3.8238	2.2612
30	0.2748	3.8443	−2.8316	2.1089	1.4798	4.1456	2.8168
35	0.4000	5.0524	−3.2064	2.7777	2.7128	3.8213	3.5793
40	0.5487	6.0467	−3.7851	3.3324	3.3564	3.9811	4.2787
45	0.7414	6.9928	−4.2489	3.8605	4.0402	4.3078	4.9227
50	0.9427	8.0483	−4.3152	4.4591	5.3715	4.5217	5.5379
60	1.3445	8.9837	−4.4358	5.2151	7.4178	4.5910	
STBR							
0	−0.0699	0.1388	0.0560	0.0055	0.0909	−0.3184	0.0055
5	−0.0642	0.6627	−0.2066	0.2636	0.0341	0.9805	0.3152
10	−0.0233	1.2475	−0.9527	0.5776	−0.2465	2.0704	0.8158
15	0.0261	1.9884	−1.8909	0.9570	−0.0784	2.7925	1.4297
20	0.0637	2.8165	−2.8234	1.4115	0.7717	3.4579	2.1174
25	0.1404	3.7948	−3.8304	1.9469	1.7263	3.8577	2.9045
30	0.2972	5.0364	−4.6474	2.5685	2.3497	3.8710	3.7303
35	0.5258	6.1106	−5.5201	3.1804	2.6822	3.8049	4.5605
40	0.8055	7.0978	−6.3448	3.7867	3.1665	2.9788	5.3729
45	1.1385	7.9944	−7.3383	4.4031	3.8329	1.7090	6.2376
50	1.4243	7.8232	−7.7925	4.6081	5.0337	2.9551	6.5562
60	1.5926	8.0708	−6.7805	4.9122	5.7005	0.9591	
EMB							
0	−0.0215	−0.0430	−0.0859	−0.0165	−0.4902	0.1017	−0.0165
5	−0.0021	0.4038	−0.3957	0.2315	−0.4612	1.9235	0.3304
10	0.0230	1.1897	−1.3214	0.5750	−0.6094	2.7714	0.9053
20	0.1723	3.0641	−3.4534	1.5420	0.9412	4.6054	2.4053
25	0.2553	4.3168	−4.5081	2.1778	1.8812	5.0206	3.3048
30	0.3254	5.6153	−5.3943	2.8162	2.6166	5.5875	4.1648
35	0.3990	6.8243	−6.3348	3.3669	3.3855	6.2552	4.9506
40	0.4860	7.9478	−6.9790	3.9001	4.6308	6.4518	5.6448
45	0.5282	8.4532	−7.1952	4.1457	5.3039	6.0778	5.9445
50	0.5243	8.4034	−7.0961	4.0928	5.3224	5.5211	5.8668
60	0.2050	6.3618	−4.3154	3.1520	0.7657	1.0481	4.2309

c_{mxlee} based on a distance between wheel-contact points of $b_a = 1.5$ m.

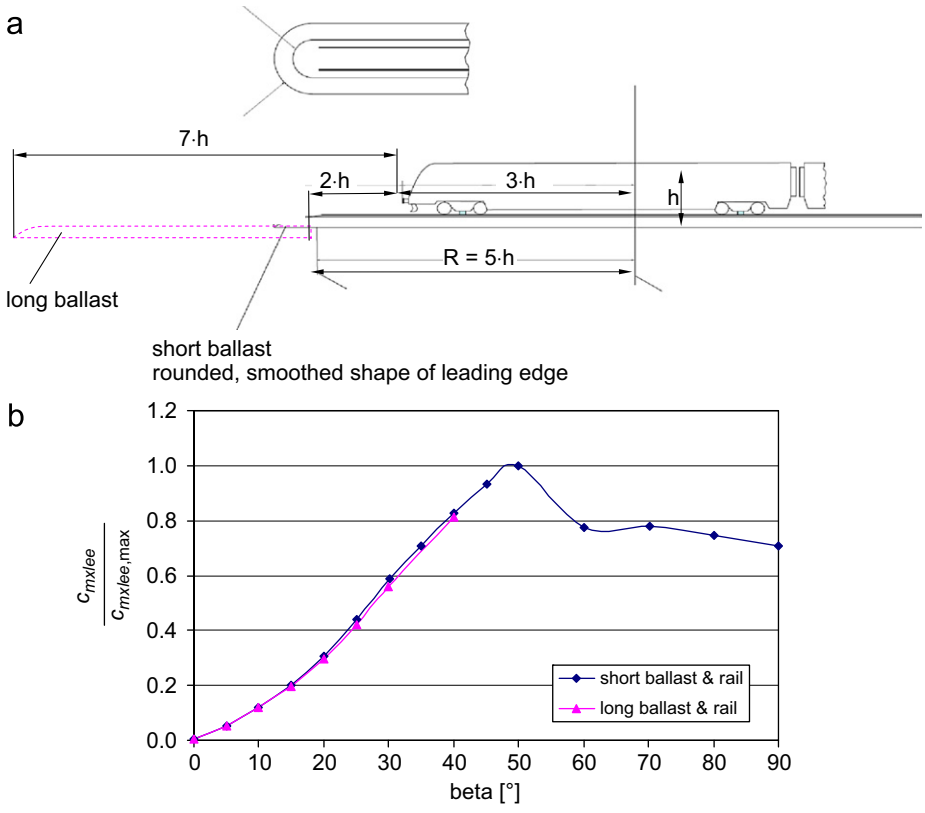

Fig. 10. Influence of upstream ballast length on lee-rail roll-moment coefficient.

References

Baker, C.J., 1985. The determination of topographical exposure factors for railway embankments. J. Wind Eng. Ind. Aerodyn. 21, 89–99.

Baker, C.J., Humphreys, N.D., 1996. Assessment of the adequacy of various wind tunnel techniques to obtain aerodynamic data for ground vehicles in cross winds. J. Wind Eng. Ind. Aerodyn. 60, 49–68.

Blakeney, A., 2000. Resistance of railway vehicles to roll-over in gales. Railway group standard, Railtrack PLC.

CEN, 2008. prEN 14067—railway applications aerodynamics—part 6: requirements and test procedures for cross wind assessment. European Norm, CEN/TC 256.

DB Netz AG, 2006. Richtlinie 80704 Aerodynamik/Seitenwind. April 2006, Deutsche Bahn.

Diedrichs, B., Sima, M., Orellano, A., Tengstrand, H., 2007. Crosswind stability of a high-speed train on a high embankment. In: Proceedings of the IMechE, vol. 221 Part F: Journal of Rail and Rapid Transit, pp. 205–225.

EC, 2006. TSI—Technical Specification for Interoperability of the trans-European high speed rail system. European Law, Official Journal of the European Communities.

Fernholz, H.-H., Janke, G., Kalter, M., Schober, M., 1993. On separated flow behind a swept backward-facing step. In: Gersten, K. (Ed.), Notes on Numerical Fluid Mechanics, 40. Vieweg, pp. 200–207.

Gawthorpe, R.G., 1994. Wind effects on ground transportation. J. Wind Eng. Ind. Aerodyn. 52, 73–92.

Orellano, A., Schober, M., 2003. On side-wind stability of high-speed trains. Vehicle Syst. Dyn. Suppl. 40, 143–160.

Orellano, A., Schober, M., 2006. Aerodynamic performance of a typical high-speed train exposed to cross-wind. In: 4th WSEAS Transactions on Fluid Mechanics, pp. 379–386.